Design and Test of an Ironless Axial Flux Permanent Magnet Machine using Halbach Array

Todd D. Batzel, Andrew M. Skraba, Ray D. Massi
Penn State University, Altoona College
tdb120@psu.edu, ams6582@psu.edu, rdm5222@psu.edu

Abstract

Conventional permanent magnet electric machines utilize ferromagnetic cores of high permeability. The high core permeability relative to the surrounding material helps to concentrate the magnetic flux in the core, and guide the flux across the airgap of the machine. An ironless machine design removes the ferromagnetic core, thus eliminating core losses due to hysteresis and eddy currents. As a result, the machine is capable of improved efficiency even at high speeds where core losses are problematic in conventional designs. The ironless design also has zero cogging torque, reduced weight, and is simple to manufacture. The axial flux implementation of this machine has been shown to have performance advantages over the radial flux machine, and also permits an adjustable airgap length.

However, the absence of an iron core generally results in lower airgap flux, which is a handicap in terms of torque production. For high torque, the airgap magnetic flux density should be as high as possible. Although this is difficult to achieve without an iron core, a Halbach array of permanent magnets can be used to focus the magnetic flux toward the airgap. The Halbach magnet array also produces a naturally sinusoidal airgap flux distribution, which helps to reduce torque torque ripple when operated with synchronous drives. The Halbach array requires additional permanent magnetic material, however, which yields higher material cost.

In the paper the design and test of an ironless axial flux permanent magnet motor are presented. The machine requirements and drive constraints (power, speed, diameter, available bus voltage) are used to size the motor. The rotor design consists of optimizing the airgap length and determining magnet dimensions. From the identified airgap length, the stator arrangement and coil design is then realized. The machine is constructed and tested, with predicted performance compared to observed experimental results.

Introduction

Traditional permanent magnet electric machines are constructed with iron core in both the rotor and stator to reduce the machine's magnetic reluctance and obtain a strong airgap flux. The continued advancement of high energy density permanent magnet materials has enabled the development of ironless electric motors [1, 2] while still maintaining a sufficient airgap magnetic flux. The elimination of iron has several advantages, including increased efficiency

due to absence of core losses [3, 4], no cogging torque [5], and light weight [6]. Due to these advantages, the ironless machine is especially attractive in applications such as high frequency energy storage flywheel [7], large [8] and small [9, 10] vehicle propulsion systems, aerospace auxiliaries [11], renewable energy systems [12], and general purpose industrial servos [13]. The drawback to the ironless motor is a typically low airgap magnetic flux density, and high current ripple resulting from the use of traditional PWM electric drives to low inductance machines such as those without iron cores [14].

Permanent magnet machine topologies are generally classified as radial flux or axial flux machines. In the common radial flux machine, the permanent magnets are arranged on the rotor (an inner cylinder) so that the torque is produced from magnetic flux that is perpendicular to the rotor shaft. In the axial flux machine [15], the magnets are arranged on a disk so that magnetic flux flowing parallel to the shaft produces the torque. The work in [16] and [17,18] shows that the axial flux design will in general result in higher specific torque and smaller volume per unit torque, respectively, than the radial machine. Although there are many variants of the axial flux machine, the topology adopted in this paper utilizes two external rotor disks sandwiched around a single internal stator. This modular topology allows several identical axial rotor stages to be stacked onto a single shaft to increase output torque as needed.

Without an iron core, a large effective airgap is unavoidable, and a higher volume of permanent magnet material is necessary to establish sufficient airgap flux. To address the low airgap magnetic flux that is typically present in an ironless machine, a Halbach array [19] is employed in this paper. An arrangement of discrete permanent magnet segments with their angle of magnetization varying with respect to the stator winding magnetic axis forms a Halbach array. A Halbach array where the permanent magnets are at 0, 90, 180, and 270 degrees from the winding is shown in Fig. 1. As shown, the magnetic field produced by the Halbach array is focused on one side of the magnetic array, and nearly zero on the other side, so that rotor backiron is unnecessary. This focusing of the field by the Halbach array is used to obtain high airgap flux (where flux is needed to produce torque) even in the absence of an iron core.

In this paper, the development and testing of an axial gap, dual-rotor single stator motor/generator is presented. The mechanical design of the machine is presented, and both the rotor and stator electromagnetic design aspects are discussed in detail. The test results will be then be used to show that the resulting air-cooled ironless design compares favorably with commercially availably iron core machines in terms of specific torque and power, torque per unit volume, and efficiency.
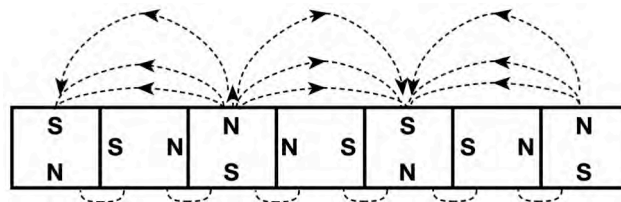

Fig. 1. Halbach magnetic array.

Machine Design

Machine Sizing: In this section, the dimensions of the axial flux ironless machine are determined. The sizing analysis begins with the design parameters and desired machine ratings, which are are summarized in Table I. The machine is being constructed mainly for laboratory experimentation and to compare the performance of an ironless machine to commercially available iron core machines in terms of efficiency, noise, specific torque and power, and torque per unit volume. However, this machine is appropriate for a variety of applications, including small vehicle propulsion, aerospace or electric vehicle auxiliaries, and small-scale wind turbines.

Table I. Machine Design Parameters

Parameter	Value
DC Bus Voltage	60 V
Torque	5.94 N-m
Base Speed	1200 RPM
Rated Current	10 A (rms)
Rated Power	1 HP
Voltage Constant	.092 $V_{phase,pk}/\omega_e$
Torque Constant	.276 N-m/A (per phase)
Poles	6
Connection	Star (Y connection)

A starting point for determining the axial machine dimensions that will allow the machine to conform to the specifications of Table I is the average airgap shear stress τ . Airgap shear stress is a measure of the torque producing force relative to the active surface area of the rotor. In general, the airgap shear stress is similar across different sizes of the same class of machines and is therefore widely used as an indicator of torque per unit volume. For an axial flux machine, the average airgap shear stress (τ) is defined as

$$\tau = \frac{T}{A_{rotor}r_{av}} \ ,$$

(1)

where T is the torque applied to the machine shaft, A_{rotor} is the active surface area where stator current is interacting with the magnetic flux, and r_{av} is the average radius of the rotor magnets. The active surface area is given by

$$A_{rotor} = \pi\left(r_o^2 - r_i^2\right) \ ,$$

(2)

where r_o and r_i are the magnet outer and inner radii, respectively, as shown in Fig. 2. Since

$$r_{av} = .5(r_o + r_i) \ ,$$

(3)

we can define the ratio of inner to outer magnet radius by

$$\alpha = \frac{r_i}{r_o} \ ,$$

(4)

and the torque is

$$T = \left(1 - \alpha^2\right)\left(1 + \alpha\right)\frac{\pi\tau}{2}r_o^3 \ .$$

(5)

The relation between outer radius and airgap shear stress can be expressed as

$$r_o = \left(\frac{2T}{\left(1-\alpha^2\right)\left(1+\alpha\right)\pi\tau} \right)^{1/3} . \tag{6}$$

Thus, the outer radius of the machine is dependent on the rated torque (from Table I), the airgap shear stress, and the ratio of inner to outer radius. Clearly, the ratio of the inner to outer radius of the machine is an important design parameter. Many studies have been performed to find the optimum ratio. In [20], the ratio was shown to be .57, while in [21] the optimum ratio was .63. In [22] the optimum ratio is shown to depend on many other design parameters such as flux density, speed, and number of poles, but was generally in a limited range near the results cited in [20] and [21]. Based on these studies, the inner to outer radius ratio α was selected to be 0.5. This value is in the narrow range cited in the studies, and is also a value that would allow a commercially available arc magnet to be obtained without the expense associated with custom magnet dimensions.

In eq. (6), the average airgap shear stress must also be selected to determine the machine radius. Airgap shear stress is generally similar for different sizes of the same class of machines [23, 24]. Of the various classes of electric machines, the permanent magnet synchronous motor (PMSM) is capable of the highest airgap shear stress. In [24] high performance industrial PMSM designs without special provisions for forced cooling have an airgap shear stress ratings in the range from 13.75 to 27.5 kPa. For the present design, the upper range of shear stress (27.5 kPa) is selected as a starting point for sizing the ironless machine. With this airgap shear stress, along with the rated machine torque, the outer diameter r_o is found to be 1.95 inches from eq (6). This was rounded up to 2 inches because of off-the-shelf magnet availability in that size. Consequently, the inner radius r_i is 1 inch.

The fundamental relationship for torque production in an axial flux permanent-magnet (PM) machine is the equation which links the force F on a wire of length l carrying a current i in a uniform magnetic field B, where the field and current are perpendicular to one another:

$$F = Bli . \tag{7}$$

Consider now the linear current density Z (in A/m), which is the total current per unit length around the airgap occupied by the stator coils. This is also often called the electrical loading of the machine. The force on the conductors can be related to the airgap shear stress and
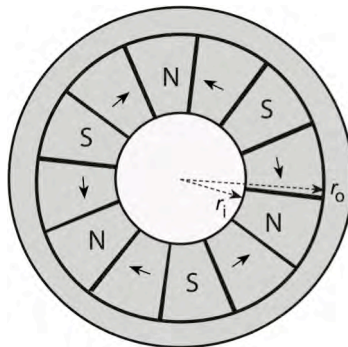

Fig. 2. Axial Dimensions

therefore to the electrical loading by

$$\tau = \frac{F}{A_{rotor}} = \frac{Bli}{lw} = \frac{Bi}{w} = BZ \quad , \tag{8}$$

where w is the average linear length around the airgap, and B is the mean airgap flux density per pole (units Teslas) – or equivalently the magnetic loading. Note that airgap shear stress is dependent on the electrical and magnetic loading points. For the sinusoidal flux density distribution, the mean airgap flux density per pole is related to the peak flux density B_m by

$$B = \frac{2B_m}{\pi} \quad . \tag{9}$$

To achieve the desired airgap shear stress of 27.5 kPa, we will choose a mean magnetic flux density B near .5 Tesla, and Z near 55,000 A/m. In the following sections, the average airgap shear stress, and hence the electrical and magnetic loading, will be used to design the stator and rotor.

Stator Design: From the sizing computations, an electrical loading (Z) of 55,000 A/m was chosen as a baseline. Now, using the electrical and magnetic loading, rated current, and dc bus voltage, the coil size and number of turns per phase of the stator may now be specified.

From the radial dimensions of the permanent magnets (r_o and r_i) the stator coil dimensions can be determined. For ease of manufacture, a non-overlapping winding is used, with 1 coil per phase for each pole pair. For the 6 pole machine, this translates to 3 coils per phase, and a total of 9 coils for the 3-phase machine. Each coil in the same phase will be connected in series, and the phases connected in a star (or "Y") configuration.

The 9 non-overlapping coils will each occupy $40°$, or 1/3 of a magnetic pole pair. The coil shape is trapezoidal, as shown in Fig. 3, with an average area enclosed by the winding of $A_{coil} = 5 \times 10^{-4} m^2$. From the DC bus operating voltage of 60V, and the star connection, each phase should develop a peak emf of $60/\sqrt{3}$ or 34.6 V at the base speed of 1200 RPM. To find the number of turns per phase N_{ph} to accomplish this, Faraday's law is used:

$$e_{ph} = N_{ph}A_{coil}\frac{dB(\theta)}{dt} \quad . \tag{10}$$

Here, e_{ph} is the per phase emf, and the flux density varies sinusoidally around the airgap according to

$$B(\theta) = B_m \sin(\omega_e t) . \tag{11}$$

The term ω_e represents the electrical frequency of the stator voltage, as determined by the shaft speed and the number of poles. At the base speed of 1200 RPM, ω_e is 377 rad/sec (or 60 Hz). From the two previous equations,

$$e_{ph} = N_{ph}A_{coil}\omega_e B_m \cos(\omega_e t) . \tag{12}$$

Thus, the number of turns per phase required to produce a peak per phase emf is given by

$$N_{ph} = \frac{e_{ph}}{A_{coil}\omega_e B_m} . \tag{13}$$

The number of turns per phase N_{ph} is determined to be 233. Since there are 3 coils per phase, each coil should have 77 turns.

For the actual coil construction, 18 gauge (round) class H magnet wire was chosen to handle the required 10 A rms, yielding an acceptable conductor current density $J= 8\ A/mm^2$. An 18 gauge conductor has a diameter of approximately 1.2 mm. Thus, to accommodate the 77 turns, the coil has a height of approximately 15 mm or .59 inches. Half of a single coil is shown in Fig. 3. Also, the total resistance per phase is computed to be $0.39\,\Omega$.

Any torque, speed, or position controller for a PMSM requires rotor position feedback. To accommodate this need, three Hall effect sensors were installed onto the stator between the phase A, B, and C coils to allow coarse rotor position detection sufficient to drive the ironless machine with trapezoidal, or six-step currents. A rotary encoder can be added to the shaft if higher resolution rotor position feedback is preferred.

The electrical loading for the stator design at the outer radius r_{av} is the product of the total number of wires (2 wires per turn) per coil, multiplied by number of coils per phase, the number of phases, and the rated current – divided by the length around the gap at that radius:

$$Z = 2m_1 N_{ph} \frac{i_{rms}}{2\pi r_{av}} , \tag{14}$$

where m_1 is the number of phases. This yields Z=58,600 A/m, which essentially meets the target electrical loading of 55,000 A/m specified in the sizing section.

Rotor Design: As shown in eq (8), the designated average airgap shear stress of 27.5 kPa can be realized by many combinations of electrical and magnetic loading. When selecting electric and magnetic loading, it is important to consider that they compete with one another for space in a fixed size machine. For example, if magnetic loading is increased by reducing the airgap length, this leaves less room for electrical conductors in the airgap, and therefore a decrease in the electrical loading. An electric loading of 55,000 A/m, and magnetic loading of approximately .5 Tesla is selected in this case to yield the targeted airgap shear stress.

Fig. 3. Stator coil.

In the machine sizing section, the rotor magnets were selected to have an inner and outer radius of 1 and 2 inches, respectively. For a 6 pole Halbach rotor disk with 4 magnets per pole pair, each magnet must have an arc of $30°$. The magnets to be used are NdFeB grade N52, with $B_r = 1.48$ T. To implement the Halbach array, half of the magnets are magnetized in axial direction, others in circumferential direction, as shown in Fig. 2.

The axial thickness of the permanent magnets can now be determined. Theoretical formulas for airgap flux density produced by Halbach magnet arrays have been developed in [25]. From these results, the airgap flux density versus gap thickness for various magnet thicknesses have been computed, and the results shown in Fig. 4. Noting that the desired mean average flux density per pole (B) of 0.5 T corresponds to a peak flux density B_m of 0.78 T, the results show that the magnetic loading can be achieved with a 1 inch thick magnet using an airgap of approximately .65 inches. Considering that the required coil thickness (from previous section) is .59 inches, this leaves very little room for clearance, coil support structure, and magnet retainers. Thus, a sacrifice in magnetic loading was made to accommodate readily available magnets of thickness 1 inch so that the prototype ironless machine could be built with adequate clearances and magnet retainers at a reasonable cost. A conservative airgap length of 1.2 inch was selected, which in theory will reduce the magnetic loading from the target of .5 T to about .39 T. It should be noted that after the machine is fully tested, the magnet retainers and stator support structures can reduced in thickness (or eliminated), and the coils re-wound with rectangular wire to enable the stator to fit into the targeted airgap of .65 inches (or even less) so that the magnetic loading target value of .5 T can be realized.

To verify the theoretical computation of the airgap flux density shown in Fig. 4, the Halbach rotor disks with magnets of 1 inch thickness were positioned for various gap lengths, with the peak airgap flux density measured using a gaussmeter. The experimentally measured peak flux density shown in Fig. 5 for various gap lengths agree very well with the theoretical results for the 1 inch magnets shown in Fig. 4. For example, in Fig. 4 a 1 inch thick magnet with a gap of 1 inch yields a theoretical peak airgap flux density of .61 T. The
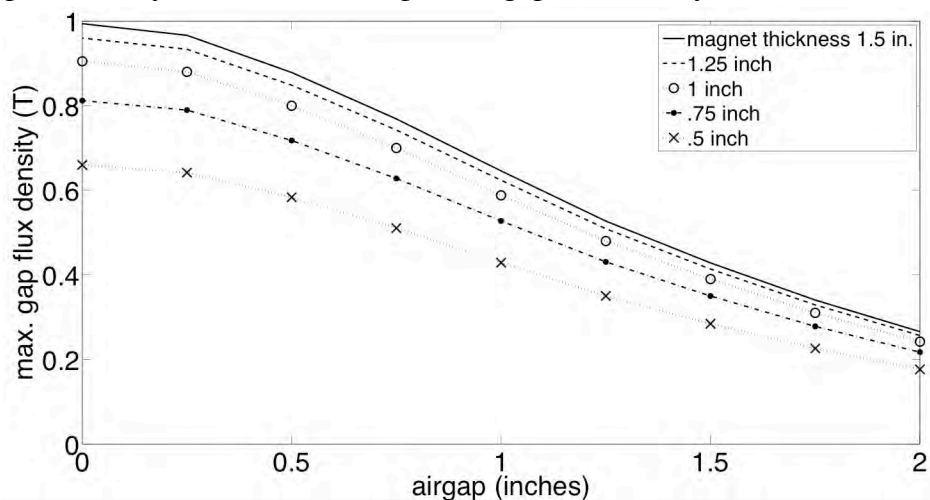

Fig. 4. Airgap flux density versus gap length for various Halbach magnet thicknesses.
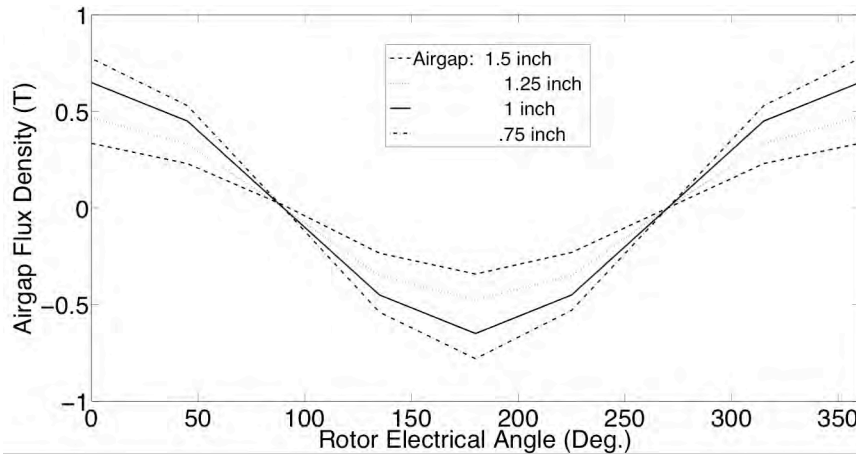
Fig. 5. Measured airgap flux density versus airgap length for 1 inch magnets.

experimentally measured peak for the same gap length, as shown in Fig. 5 was found to be .64 T.

Machine Construction and Testing

The rotor PM disks were designed using Solidworks. The magnet disk was constructed with aluminum for light weight. Since the aluminum disk rotates with the magnets, it does not see a changing magnetic flux and therefore will not be subject to significant eddy current losses. The Solidworks implementation of a single Halbach magnet disk, showing the magnet locations, is shown in Fig. 6.

In the ironless motor design, two magnet disks will be sandwiched around the stator such that the Halbach array focuses the magnetic field to the airgap between the disks. The full assembly – minus the stator – is shown in Fig. 7. The stationary end bells shown in the figure are also constructed with aluminum, and hold bearings to accommodate the rotating shaft. The magnet disks are fixed to the keyed shaft with a shaft collar and keystock. Note also that the airgap length (axial distance between the magnets) is easily adjustable. The stator (not shown) is held fixed to the end bells using screws and spacers of appropriate length. The actual Halbach rotor disk is shown in Fig. 8.
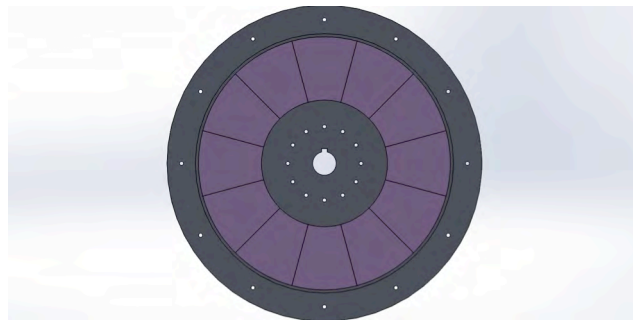

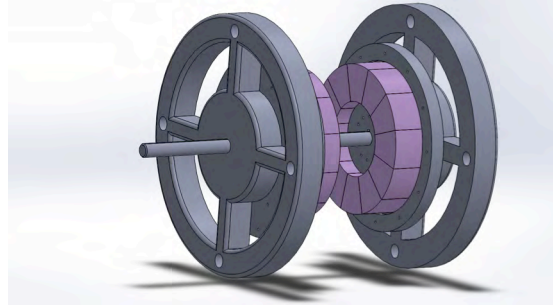Fig. 6. Solidworks design of rotor magnet disk.

Fig. 7. Dual rotor disks on shaft, with endbells.

Fig. 8 Rotor disk with Halbach array.

The stator was constructed by mounting the coils onto a supporting acrylic sheet of thickness 3/32 inch. Each coil, as presented in the previous section has a total of 77 turns. In practice, this was accomplished with two separate coils of 38 turns mounted to opposite sides of the stator support structure, and connected in series. The constructed stator assembly is shown in Fig. 9, and the fully constructed ironless axial flux machine in Fig. 10.

As indicated in Table I, the voltage constant of the machine k_e is the computed ratio of the peak phase voltage relative to the electrical frequency. From the design parameters, the per phase peak voltage at rated speed is 34.6 V, since the maximum line-to-line voltage is limited
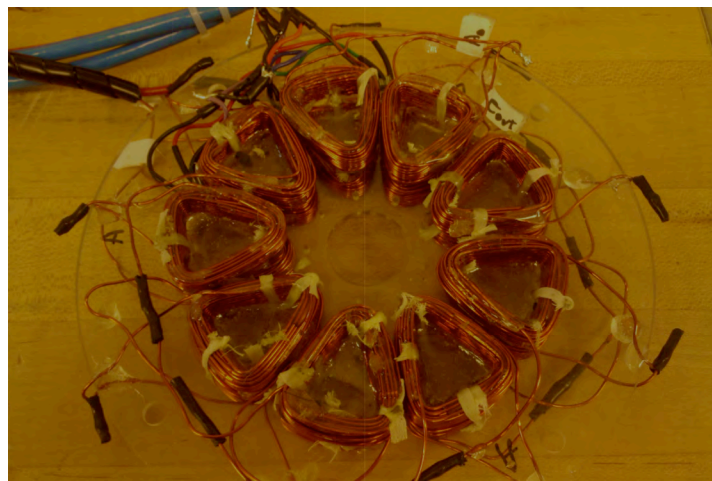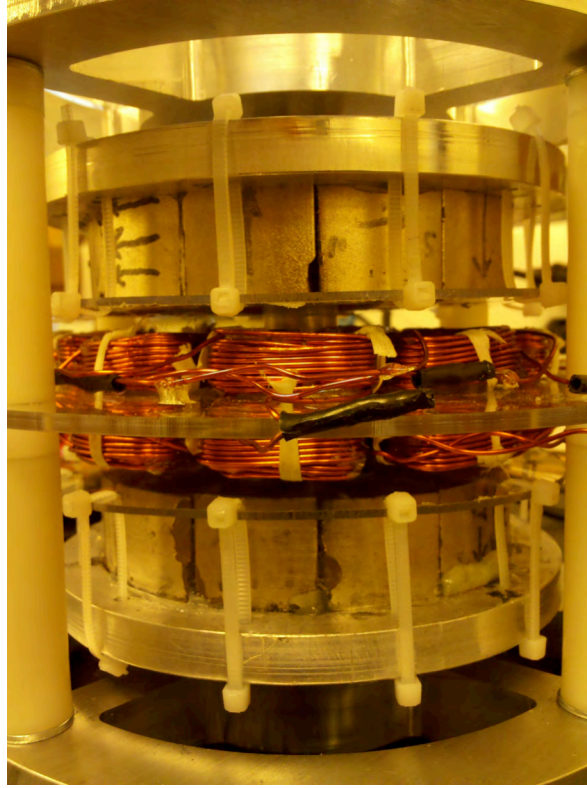

Fig. 9. Stator Assembly.

Fig. 10. Constructed Ironless Axial Flux Motor.

by the DC bus voltage of 60 V. The electrical frequency at 1200 RPM is 377 rad/s, so the voltage constant k_e is .092 v-s. For the torque constant k_t, the number of pole pairs (3 for the machine of interest) must be considered, so the torque constant is k_t is .276 N-m/A per each phase. Assuming the drive enforces optimum commutation angle using the rotor position feedback θ_e, the total machine torque is obtained from the instantaneous phase currents:

$$T = k_t \left(i_a \sin\theta_e + i_b \sin\left(\theta_e - 120^\circ\right) + i_c \sin\left(\theta_e + 120^\circ\right) \right). \tag{15}$$

For sinusoidal current excitation, the torque will ideally be constant, with no ripple.

TESTING: For the machine testing, the ironless machine was placed on a motor test dynamometer, as shown in Fig. 11. The first test that was performed was to determine the voltage constant k_e, which was computed earlier to be .092 v-s. To experimentally determine the voltage constant, the machine was driven as a generator with the induced phase voltages recorded, as shown in Fig. 12. Note in the figure that the induced voltages are sinusoidal with the 3-phase voltages balanced. The peak voltage in is seen to be 6.15 volts, and the electrical frequency is 20π rad/sec. The voltage constant k_e is .098 v-s, which agrees well with the value computed in the previous section of .092 v-s.
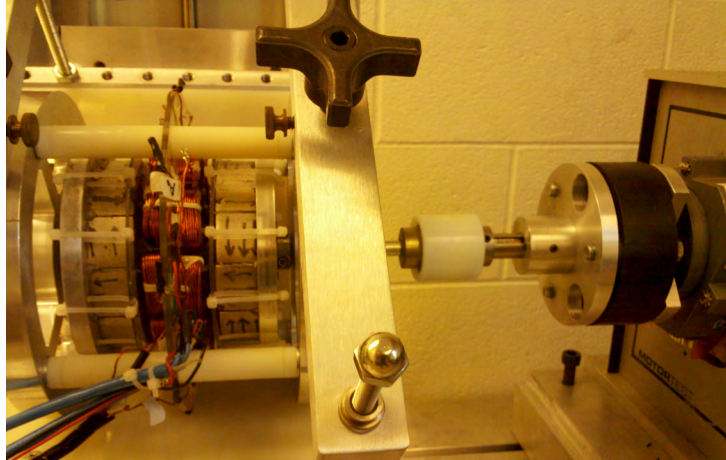
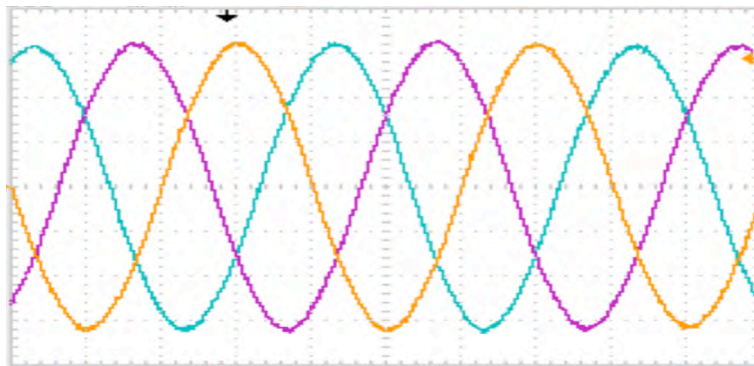Fig. 11. Ironless motor coupled to dynamometer on motor test stand.

Fig. 12. Back EMF waveform (2 V div, 25 ms/div).

The torque versus speed characteristic of the machine was obtained by placing the ironless machine on a dynamometer, while measuring shaft torque and RPM. For the tests, the stator current was limited to 10 A rms per phase due to thermal constraints. Likewise, the rotor speed was limited to 1200 RPM for several reasons: the DC bus voltage would need to be increased for higher speed, and the centrifugal force F_c on the magnets increases in proportion to speed squared:

$$F_c = mr\omega^2 . \tag{16}$$

At 1200 RPM, approximately 13 lbs. of centrifugal force is acting on each magnet, whose mass is .0975 kg. Until the adhesive used to bond the magnets to the disk is qualified for higher forces, rotational speed shall limited to 1200 RPM. The obtained torque versus speed characteristic is shown in Fig. 13. Note that the experimentally obtained torque is in good agreement with the expected value. For example, with the shaft angle at $\theta_m = 90^\circ$ and the instantaneous phase currents of $i_a = 14.14$ A, $i_b = -7.07$ A, and $i_c = -7.07$ A, the theoretical torque, from eq. (15) should be 5.85 N-m.
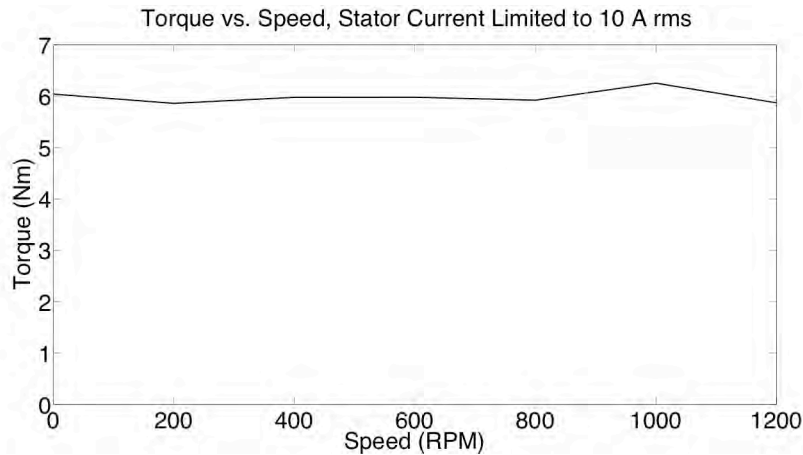
Fig. 13. Torque vs. Speed.

Next, the machine efficiency was experimentally determined for various operating points. In each case, the input (electrical) power was determined from measured phase voltages and currents. The output power was obtained from measured shaft torque and speed. For this experiment, a fan type load was assumed, where load torque is proportional to the speed squared. The applied load torque versus speed curve used is shown in Fig. 14. Efficiency versus speed results are above 90% over a wide range of speed, as shown in Fig. 15.

Efficiency tests reveal that the machine delivers 1 HP at 1200 RPM as expected. Additional qualification of the magnet adhesive may allow power rating increases by running the machine at higher speed, without the core losses associated with iron core machines. The total weight of the machine is 4.8 kg, which yields a power to weight ratio of 156 W/kg. Comparison to commercial machines of the same rating are difficult because the required data is only available from data sheets, and maximum versus short-time power ratings are not always clearly defined. Machines in the same power range with convection cooling must be used as comparison because the specific power (W/kg) tends to increase with the machine power rating. For comparison, specifications from several vendors' iron core PM machines in the range of 1 HP were examined. The specific power of those machines ranged from 64 W/kg up to 177 W/kg. Thus, the prototype ironless machine, even without serious consideration to weight reduction, compares well with those commercial iron core machines.
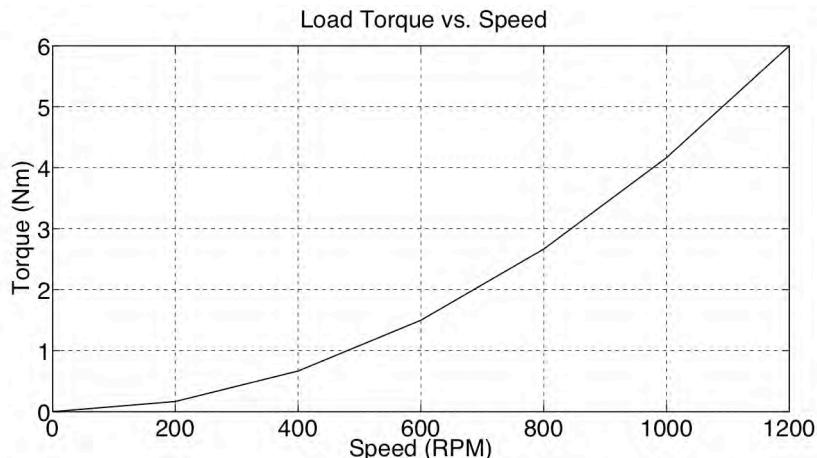

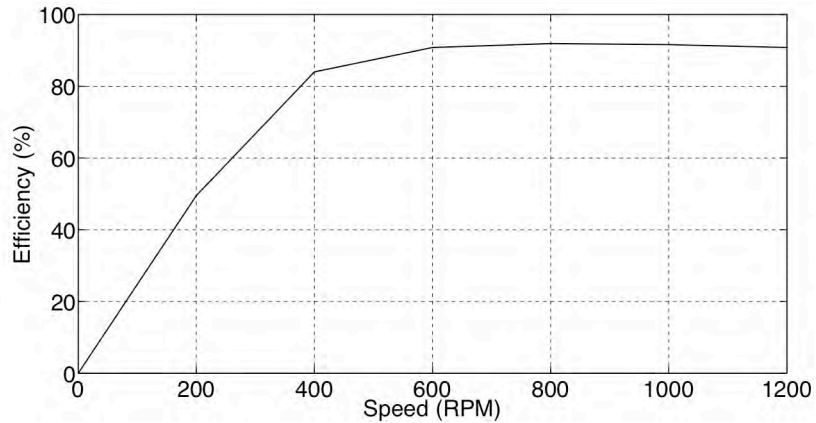Fig. 14. Load torque versus speed characteristic used for efficiency tests

Fig. 15. Ironless machine efficiency for pump load where torque proportional to speed[2].

The power density (power per unit volume) of the ironless design was also compared to the commercial iron core machines. The ironless machine was found to have a power density of 505 kW/m^3. The commercial iron core machines that were examined had power densities ranging from a low of 375 kW/m^3 to 525 kW/m^3. Thus, the power density of the ironless machine compares well with those commercial machines.

Conclusion

The design of an ironless axial flux electric machine is presented. The design is carried out starting with basic design goals and constraints, and by using motor sizing estimates. For the rotor, a Halbach magnet array is used to concentrate flux in the airgap of the machine. This choice enables reasonable magnetic loading even in the absence of an iron core, while maintaining sufficient airgap length for aggressive electric loading. The proposed machine design is then constructed and tested, with results showing excellent efficiency of well over 90% across a large operating range. The proposed design is also shown to be on par with many commercially designed machines of the same power rating in terms of power density and specific power rating. With additional attention to the magnet bonding to the rotor disc, the rated machine speed (and therefore power) can be increased to further improve power density without incurring additional inefficiencies that are unavoidable with iron core designs. The results suggest that the ironless machine is easily manufactured, and is a viable alternative to iron core designs – especially in applications where high speed, high efficiency, and low cogging torque are essential.

References

[1]   Profumo, F., F.J. Eastham, A. Tenconi, G. Gianolio, "Plastic electric motors: a viable solution for axial flux machines," *Proceedings of the 2002 IEEE International Symposium on Industrial Electronics*, vol. 1, 2002. pp. 1-10.

[2]   Lovatt, H.C., V.S. Ramsden, and B.C. Mecrow, "Design of an in-wheel motor for a solar-powered electric vehicle," *Eighth International Conference on Electrical Machines and Drives*, 1997. pp. 234-238.

[3]   Kamper, M.J., Wang, R.-J., Rossouw, F.G.: 'Analysis and performance of axial flux permanent-magnet with air-cored non-overlapping concentrated stator windings', *IEEE Trans. Ind. Appl.*, 2008, 44, (5),pp. 1495–1504.

[4]   J.F. Gieras, Gieras, I.A., "Performance analysis of a coreless permanent magnet brushless motor," *Conference Record of the 37th IAS Annual Meeting, Industry Applications Conference*, vol. 4, 2002. Pp. 2477-2485.

[5]   Praveen, R.P., M.H Ravichandran, V.T.S. Achari, V.P.J. Raj, G. Madhu, and G.R. Bindu, "Design and analysis of zero cogging Brushless DC motor for spacecraft applications," *International Conference on Electrical Engineering/Electronics Computer Telecommunications and Information Technology (ECTI-CON)*, 2010. pp. 254-258.

[6]   O. Winter, S. Ucsnik, M. Rudolph, C. Kral, E. Schmidt, "Ironless in-wheel hub motor design by using multi-domain finite element analyses," *International Symposium on Power Electronics, Electrical Drived, Automation and Motion (SPEEDAM)*, 2012, pp. 1474-1478.

[7]   Colotti, A, O. Garcia, B. Ronner, and K. Reichart, "Design of an ironless PMSM for flywheel storage systems," *International Conference on Electric Machines (ICEM)* 1998, v. 2, pp. 1128-1133.

[8]   Ren, X., and Z. Wang, "Multi-stage PM disc motor for ship propulsion application," *Sixth International Conference on Electrical Machines and Systems (ICEMS)*, vol. 1. 2003. Pp. 52-55.

[9]   Stamenkovic, I., N. Milivojevic, M. Krishnamurthy, N. Schofield, A. Emadi, "Ironless Machine Design and Novel Digital Control for Automotive Applications," *IEEE Vehicle Power and Propulsion Conference*, 2009. pp. 475-480.

[10]   Al Zaher, R. S. de Groot, H. Polinder, P. Wieringa, *International Conference on Electrical Machines (ICEM)*, 2010. Pp. 1-6.

[11]   De, S., M. Rajne, M. Poosapati, C. Patel, K. Gopakumar, "Low-inductance axial flux BLDC motor drive for more electric aircraft," *IET Power Electronics Journal*, vol. 5, no. 1. 2012. pp. 124-133.

[12]   Bumby, J.R., and R. Marting, "Axial-flux permanent-magnet air-cored generator for small-scale wind turbines," *IEE Proceedings on Electric Power Applications*, vol. 152, n. 5, 2005, pp. 1065-1075.

[13]   Kessinger, R.L., and S. Robinson, "SEMA-based permanent magnet motors for high-torque, high-performance," *Proceedings of the Naval Symposium on Electric Machines Conference*, 1997, pp. 151-155.

[14]   Batzel, T.D., K. Adams, "Variable Timing Control for ARCP Voltage Source Inverters Operating at Low DC Voltage," *International Journal of Modern Engineering* (IJME), v. 13, no. 2, 2013.

[15]   Price, G.F., T.D. Batzel, B.A. Muller, M.U. Comanescu, "Design and Testing of a Permanent Magnet Axial Flux Wind Power Generator," *International Journal of Modern Engineering* (IJME), v. 9, no. 2, 2009.

[16]   Z. Zhang, F. Profumo, A. Tenconi, "Axial-flux versus radial-flux permanent-magnet motors," *Electromotion*, vol. 3, 1996, pp. 134-140.

[17]   Sitapati, K., K. Krishnan, "Performance Comparisons of Radial and Axial Field, Permanent Magnet, Brushless Machines," *IEEE Transactions on Industry Applications*, vol. 37, no. 5, Sept./Oct. 2001. pp. 1219-1226.

[18]   Patterson, D.J., C.W. Brice, R.A. Dougal, and D. Kovuri, "The 'Goodness' of Small Contemporary Permanent Magnet Electric Machines," *IEEE International Electric Machines and Drives Conference*, 2003, vol. 2, pp. 1195-2000. June 2003.

[19]   Ofori-Tenkorrang, J., and J.H. Lang, "A comparative analysis of torque production in Halbach and conventional surface-mounted permanent magnet synchronous motors," *Conference Record of the IEEE Industry Applications Conference*, *Thirtieth IAS Annual Meeting*, 1995, vol. 1, pp. 657-663.

[20]   P. Campbell, "Principle of a Permanent Magnet Axial Field DC Machine," *Proceedings of the Institute of Electrical Engineering*, vol. 121, n. 12, Dec. 1974, pp. 1489-1494.

[21]   Patterson, D.J., J.L. Colton, B. Mularcik, B.J. Kennedy, S. Camilleri, R. Rohoza, "A Comparison of Radial and Axial Flux Structures in Electrical Machines," *IEEE International Electric Machines and Drives Conference (IEMDC)*, May 2009, pp. 1029-1035.

[22   Huang, S. ,J. Luo, F. Leonardi, T.A. Lipo, "A Comparison of Power Density for Axial Flux Machines Based on General Purpose Sizing Equations," *IEEE Transactions on Energy Conversion*, vol. 14, n. 2, June 1999 pp. 185-192.

[23]   J.G. West, "DC, Induction, Reluctance and PM Motors for Electric Vehicles," *IEE Power Division Colloquium on Motors and Drives for Battery Powered Propulsion*, London, April 1993, pp. 1/1-111.

[24]   T.J.E. Miller, "*Speed's Electric Motors: An Outline of Some of the Theory in the Speed Software for Electric Machine Design*" Magna Physic Publishing, Lebanon, OH, 2006.

[25]   O.Winter, Kral, C., and Schmidt, E., "Design study of magnet shapes for axial Halbach arrays using 3D Finite Element Analyses," *IEEE International Conference on Electric Machines (ICEM)*, 2012, pp. 2660-2665.

Biographies

TODD BATZEL received the B.S. and Ph.D. degrees in electrical engineering from the Pennsylvania State University, University Park, in 1984 and 2000, respectively, and the M.S. degree in electrical engineering from the University of Pittsburgh, Pittsburgh, PA, in 1989. Currently, he is a Professor of Electrical Engineering at Penn State University, Altoona College. Dr. Batzel may be reached at tdb120@psu.edu.

ANDREW SKRABA is presently a Senior level undergraduate student in the B.S. in electro-mechanical engineering technology at Penn State Altoona, Altoona, PA. He may be reached at ams6582@psu.edu.

RAY MASSI is presently a Junior level undergraduate student in the B.S. in electro-mechanical engineering technology at Penn State Altoona, Altoona, PA. He may be reached at rdm5222@psu.edu.